

## Direct Probing of Transient Photocurrent Dynamics in p-WSe<sub>2</sub> by Time-Resolved Scanning Tunneling Microscopy

Shoji Yoshida, Yasuhiko Terada, Munenori Yokota, Osamu Takeuchi, Yutaka Mera<sup>†</sup>, and Hidemi Shigekawa\*

Graduate School of Pure and Applied Sciences, University of Tsukuba, Tsukuba, Ibaraki 305-8571, Japan

E-mail: hidemi@ims.tsukuba.ac.jp

Received November 22, 2012; accepted December 13, 2012; published online December 28, 2012

We have carried out time-resolved scanning tunneling microscopy on a layered semiconductor with an indirect bandgap, p-WSe<sub>2</sub>, and the dynamics of nonequilibrium photocurrent generated by ultrashort-pulse-laser excitation was analyzed. The photocurrent dynamics reflecting the flow of excited photocarriers at the surface, which is determined by the balance between the diffusion and tunneling rates, was successfully probed. Furthermore, the excess minority carriers transiently trapped at the surface for a few nanoseconds, which produce a transient surface photovoltage and cannot be detected by conventional methods, were directly observed and evaluated.

© 2013 The Japan Society of Applied Physics

The development of semiconductor physics and devices in the past few decades has been progressing along with the innovations, in atomically controlled fabrication technologies. With the reduction of dimensions, the characterization of performances on the nanoscale has become ever more crucial for the further development of functional materials and devices. Owing to their characteristics, scanning tunneling microscopy/spectroscopy (STM/STS) and related techniques are promising; therefore, attractive methods based on their characteristics have been developed to realize the analysis of local information, such as dopant profile, carrier distribution, local conductivity, potential variations, surface photovoltage (SPV), and local spin effects.<sup>1–6)</sup> To obtain a complete understanding of such functions, however, the analysis of carrier dynamics under a nonequilibrium state is important, and significant effort has been devoted to realize time-resolved (TR) microscopy/spectroscopy.<sup>7,8)</sup>

Recently, a new microscopy technique, shaken-pulse-pair-excited STM (SPPX-STM), which enables the probing of ultrafast carrier dynamics in nanometer-scale structures has been developed.<sup>9)</sup> The high spatial resolution of STM has been combined with the temporal resolution of an ultrashort-pulse laser in the femtosecond range on the basis of the optical pump–probe (OPP) method. A nonequilibrium carrier distribution is generated by ultrashort laser pulses and its relaxation processes are probed using the STM tunneling current. By applying the method to GaAs-based structures, fundamental carrier dynamics in semiconductors, such as photocarrier recombination and the effect of the inner potential on carrier dynamics, were successfully probed and visualized.<sup>9–11)</sup> To increase the generality of this method of microscopy and its applicability to various types of materials and structures, additional techniques are desired. For example, as an application of TR-STM based on a similar method to the analysis of a molecular electronic structure, two-photon absorption measurement was used together with TR-STM.<sup>12)</sup> For further advancement, the development of direct techniques for detecting photocurrent in transient dynamics on the nanoscale is expected to play an important role in determining the optical characteristics of materials and devices.

In this study, we have carried out SPPX-STM measurements on the transient photocurrent dynamics in a layered

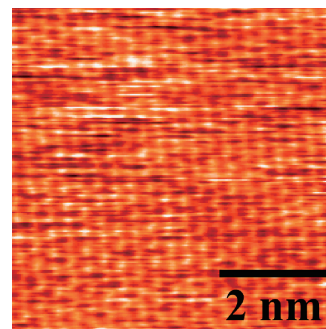


Fig. 1. Typical STM image of WSe<sub>2</sub> (set point:  $V_s = +2.0$  V,  $I_t = 100$  pA,  $5.75$  nm  $\times$   $5.75$  nm).

semiconductor, WSe<sub>2</sub>. Layered compounds have attracted fundamental and practical interest in various fields. In addition to the current interest in device applications, for example, field-effect transistors,<sup>13–15)</sup> layered materials can be used as a model system for the analysis of carrier dynamics because of their advantageous surfaces with minimal roughness, dangling bonds and defect states. Among the layered materials, the tunneling characteristics of photocurrent in the stationary state are well understood for WSe<sub>2</sub>,<sup>16,17)</sup> which allows detailed analysis of the results obtained for transient properties.

Figure 1 shows a typical STM image of WSe<sub>2</sub>. As expected, the surface is stable and no atomic scale defects<sup>18)</sup> were observed in the measurement area, even after laser excitation. First, we obtained current to bias voltage ( $I$ – $V$ ) curves by measurement using the light-modulated STS method<sup>2,3)</sup> to examine the characteristic properties of photocurrent in the stationary state. Ti:sapphire laser pulses with a pulse width of 140 fs (central wavelength, 800 nm; average intensity, 1 W, and 0.35 mW intensity at the sample) and a repetition rate of 90 MHz were chopped at 100 Hz, and two  $I$ – $V$  curves with and without laser excitation were obtained simultaneously. Under these conditions, the results were the same as those obtained with a continuous laser. A fresh WSe<sub>2</sub> surface was prepared by exfoliating a lightly p-doped sample, and measurements were carried out in air and vacuum ( $<5.0 \times 10^{-8}$  Pa), both of which produced the same results because of the high stability of the sample surface.

Figure 2 shows the results, where blue and red lines indicate the  $I$ – $V$  curves obtained without and with laser

<sup>†</sup>On leave from Department of Applied Physics, The University of Tokyo.

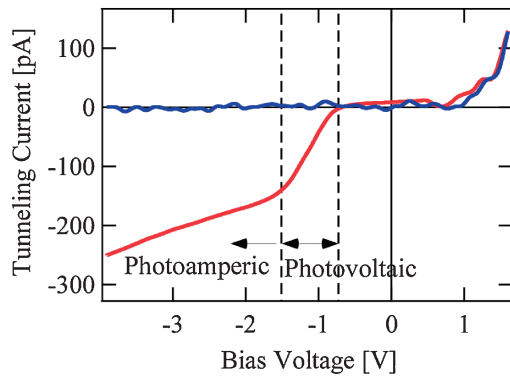


**Fig. 2.**  $I$ - $V$  curves obtained by light-modulated STS without (blue) and with (red) photoillumination (set point:  $V_s = 1.5$  V,  $I_t = 100$  pA).

excitation, respectively. A large difference was observed between the two cases. Figure 3 shows schematics of the metal-insulator-semiconductor (MIS) structures used to explain the observed results. For a positive bias voltage (forward bias voltage), the characteristic of conductivity with illumination (not shown) is the same as that under the dark condition [Fig. 3(a)], because photoelectrons drift to the bulk side. In contrast, for a negative sample bias voltage (reverse bias voltage), since electrons photoexcited in the conduction band induce tunneling, different characteristics are observed under the dark [Fig. 3(b)] and photoexcited [Figs. 3(c) to 3(f)] conditions. Here, Figs. 3(c) and 3(d) and Figs. 3(e) and 3(f) represent the time evolutions of the excited states induced by a pump pulse with a low and high intensity, respectively. The band structure appearing under illumination with a continuous laser can also be represented by Fig. 3(e) or 3(f).

Let us consider the case of a negative sample bias voltage in more detail. Under the dark condition [Fig. 3(b)], minority carriers, i.e., electrons, at the surface conduction band of  $\text{WSe}_2$  provided from the bulk side are extracted by tunneling into the STM tip instead of accumulating. Therefore, an inversion layer is not formed, resulting in downward bending of the surface Fermi level of  $\text{WSe}_2$ . This nonequilibrium change induces a large amount of tip-induced band bending (TIBB) and prohibits electron tunneling from the valence band of  $\text{WSe}_2$ , producing the observed strong rectification (blue line in Fig. 2).

Under an illuminated condition using a continuous laser, the negative sample bias-voltage region is divided into two parts, as can be observed in the  $I$ - $V$  curve in Fig. 2: (1) a photovoltaic region ( $-1.5 \leq V_s \leq -0.8$  V in Fig. 1,  $V_s$ : sample bias voltage) and (2) a photoamperic region ( $V_s \leq -1.5$  V in Fig. 1). Until the conduction band edge reaches the Fermi level (photovoltaic region), the bias voltage is mainly applied to the tunnel gap, therefore, under photoillumination, the SPV, and thereby the tunneling current, strongly depends on the bias voltage. When the negative bias voltage is further increased, the tunneling gap conductance becomes higher than that in the space charge region of  $\text{WSe}_2$  owing to the reduction of the tunneling barrier height for electrons (photoamperic region). Under such a condition, the tunneling current mainly consists of photogenerated carriers from the bulk side which accumulate beneath the STM tip. Therefore, the photocurrent depends on

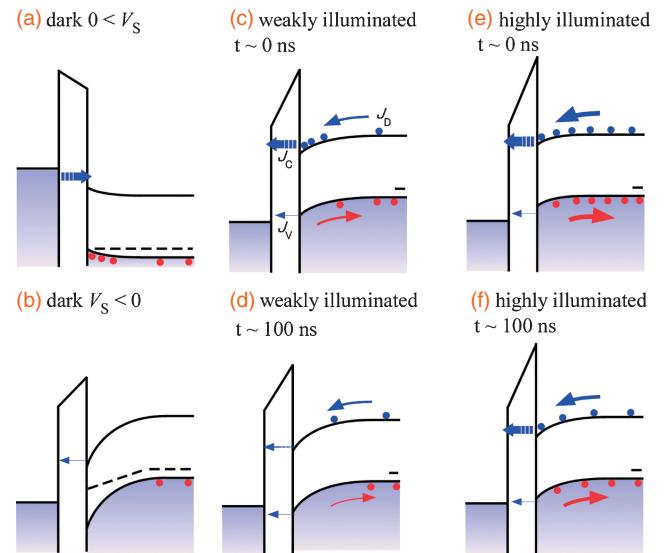


**Fig. 3.** Schematic illustrations of band structures: (a) and (b) are for positive and negative sample bias voltages under the dark condition, respectively, while (c) and (d), and (e) and (f) represent the time evolutions of the excited states induced under a negative sample bias voltage by a pump pulse with a low and high intensity, respectively.  $J_D$ : diffusion current,  $J_V$ : current from valence band,  $J_C$ : photocurrent of minority carriers. Since bandgap of  $\text{WSe}_2$  is  $\sim 1.2$  eV,  $J_V$  is negligible compared with  $J_C$ .

the photointensity and volume of TIBB, where photogenerated carriers drift toward the STM tip. Since the region of TIBB gradually increases as the bias voltage increases, the tunneling current slowly increases with the bias voltage. These results are in good agreement with those reported in a previous paper.<sup>16,17)</sup> No current is observed for a negative bias voltage under the dark condition, indicating that the photocurrent is directly detected as a signal via tunneling, making it suitable for SPPX-STM measurement and analysis.

To analyze the dynamics of the photocurrent measured in the stationary state shown in Fig. 2, we carried out SPPX-STM measurement to obtain information on the photocarrier dynamics in the temporal space. In SPPX-STM, the sample surface below the STM tip is excited by a sequence of paired pulses, similarly to the conventional OPP method, and the change in the tunneling current is measured as a function of the delay time between the pump and probe pulses. A paired laser-pulse train was generated by two synchronized Ti:sapphire lasers used above. The repetition rate was reduced to 1 MHz with a pulse picker system using pockels cells. The delay time was modulated at 1 kHz for the lock-in detection of the weak signal. The detected signal is  $\Delta I = I(t_d) - I(\infty)$ , where  $I(t_d)$  and  $I(\infty)$  are the tunneling currents for a delay time of  $t_d$  and a delay time sufficiently long for the excited state to be relaxed, respectively. Therefore, the observed change in  $\Delta I$  directly provides information about the dependence of the photocarrier density on the delay time after photoexcitation.<sup>11)</sup>

Figure 4 shows a series of SPPX-STM spectra obtained for different laser intensities. To enhance the effect of SPV to increase the magnitude of the signal, measurement was carried out under a photovoltaic condition ( $V_s = -1.5$  eV) in consideration of the result in Fig. 2. The original laser intensity was 0.9 mW, which was reduced to  $I_L$  using filters.

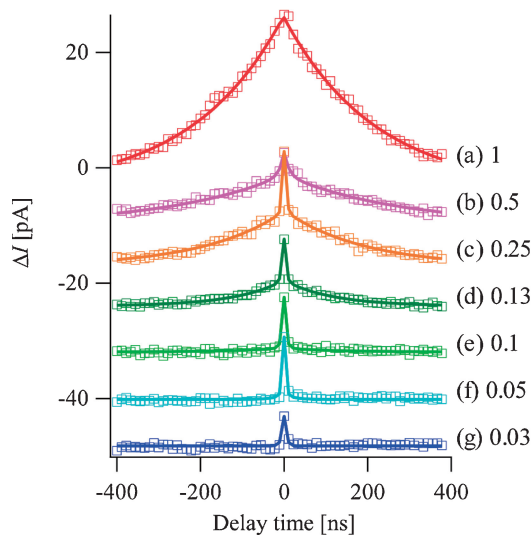


**Fig. 4.** Time-resolved spectra obtained under various laser intensities  $I_L$  (set point:  $V_s = -1.5$  V,  $I_t = 1$  nA). The maximum laser intensity was 0.9 mW and the relative intensities were (a) 1, (b) 0.5, (c) 0.25, (d) 0.13, (e) 0.1, (f) 0.05, and (g) 0.003.

A fast component (decay constant  $\sim 5$  ns) and a slow component (decay constant  $\sim 200$  ns) were observed. For low laser intensities, only the fast component appears and the intensity of the slow component increases with increasing laser intensity.

Since  $\text{WSe}_2$  has an indirect bulk bandgap, the recombination lifetime of photoexcited carriers is significantly long ( $\sim 10$   $\mu\text{s}$ ) compared with the observed values. Therefore, a possible explanation for the obtained results is that the observed dynamics in the signal reflects the change in photo-carrier (minority carrier) density with the balance between the two processes at the surface, namely, the diffusion rate of photoexcited electrons from the bulk side,  $R_d$ , and their tunneling to the STM tip  $R_t$ . In fact, the decay constant of  $\sim 200$  ns was observed by the OPP method, which supports that the process is considered to be diffusion of photocarriers from the illuminated area.

When the tip-sample distance is fixed ( $R_t = \text{constant}$ ), the photocarrier density varies with the laser intensity, and the associated change in the diffusion rate  $R_d$  governs the balance. For a low laser intensity ( $R_t \gg R_d$ ), the diffusion rate becomes the limiting factor in the balance, where the tunneling of the excess electrons trapped at the surface during photoexcitation is detected dominantly as the signal [fast component, (e)–(g) in Fig. 4]. In contrast, for a high laser intensity ( $R_t \ll R_d$ ), the tunneling rate becomes the limiting factor and the diffusion process produces tunneling with a large decay constant [slow component, (a) in Fig. 4]. In the intermediate range ( $R_t \sim R_d$ ), the excess electrons trapped at the surface first undergo tunneling. Then, electrons provided from the bulk side undergo tunneling at a rate of  $R_d$ . As a result, the slow component appears in the time-resolved spectra following the fast component [(b)–(d) in Fig. 4]. Since the signal detection is based on the mechanism of absorption bleaching similarly to the OPP method,<sup>9)</sup> the signal intensity increases with increasing the laser power.

To analyze the process for the fast component in more detail, we measured the tunneling current dependence of the

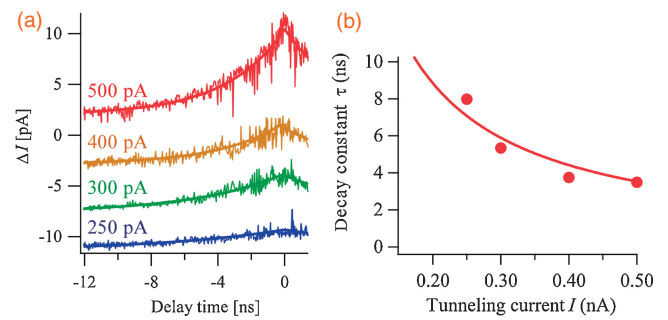


**Fig. 5.** (a) Time-resolved spectra obtained for the fast component under various laser intensities (set point:  $V_s = -2.0$  V, laser intensity: 0.2 mW). (b) Decay constant  $\tau$  obtained from (a) as a function of the tunneling current  $I_t$  adjusted by changing the tip-sample distance. The solid line indicates the fitting curve of the data with the function  $\tau = 18/I_t$ .

fast component. To observe the fast component easily, in consideration of the results in Figs. 2 and 4, measurement was carried out under the conditions of  $V_s = -2.0$  V and  $I_L = 0.2$  mW. Figure 5(a) shows the series of spectra obtained, and the decay constant  $\tau$  as a function of the tunneling current is summarized in Fig. 5(b). The tunneling current was adjusted by changing the tip-sample distance before each measurement under illumination with the pulse laser. The decay constant  $\tau$  decreases with increasing tunneling current as expected.

In the stationary-state measurement of photocurrent, as described in a previous paper, the excess electrons, which cause, for example, the inversion layer, cannot be observed because they disappear as a result of tunneling.<sup>16,17)</sup> In SPPX-STM, the number of excess electrons transiently trapped at the surface can be observed via the dynamics of the fast component. As a rough estimation, the maximum value of  $\Delta I$  gives the number of excess electrons induced by a pair of laser pulses at 1 MHz. Therefore, the number of excess electrons induced by a laser pulse is estimated to be 5–40 from the results shown in Fig. 5(a). The increase in the number of excess electrons with decreasing tip-sample distance may be caused by the increase in the area of the depletion layer produced by TIBB. These values are comparable to the number of charges  $N$  estimated to exist between a sphere of radius  $R$  and an infinite plane placed at a distance of 1 nm from the sample;  $N = 15.5$  for  $R = 10$  nm and 40.4 for  $R = 20$  nm.

In conclusion, we have carried out time-resolved STM on a p-type layered semiconductor with an indirect transition band structure,  $\text{WSe}_2$ . The photocurrent dynamics reflecting the flow at the surface, which was locally balanced between the diffusion and tunneling rates, was successfully probed. The dynamics of the excess electrons trapped at the surface, which produce a transient surface photovoltage on the nanosecond scale and cannot be detected by conventional methods, was observed and evaluated. Although we carried out measurements on the sample surfaces without defects to develop a solid basis for the new technique, the effect of nanostructures on the photocurrent plays an essential role in determining the optical characteristics of materials and devices. SPPX-STM, for example, with the manipulation techniques of STM<sup>19)</sup> may create exciting new possibilities for further studies.

**Acknowledgment** Support by the Japan Society for the Promotion of Science through Grants-in-Aid for Scientific Research is acknowledged.

- 1) M. Nishizawa, L. Bolotov, and T. Kanayama: *Appl. Phys. Lett.* **90** (2007) 122118.
- 2) S. Yoshida, Y. Kanitani, R. Oshima, Y. Okada, O. Takeuchi, and H. Shigekawa: *Phys. Rev. Lett.* **98** (2007) 026802.
- 3) S. Yoshida, Y. Kanitani, O. Takeuchi, and H. Shigekawa: *Appl. Phys. Lett.* **92** (2008) 102105.
- 4) S. Grafström: *J. Appl. Phys.* **91** (2002) 1717.
- 5) M. A. Topinka, B. J. LeRoy, R. M. Westervelt, S. E. J. Shaw, R. Fleischmann, E. J. Heller, K. D. Maranowski, and A. C. Gossard: *Nature* **410** (2001) 183.
- 6) J. Brede, B. Chilian, A. A. Khajetoorians, J. Wiebe, and R. Wiesendanger: in *Handbook of Spintronics*, ed. D. Awschalom, J. Nitta, and Y. Xu (Canopus Academic Publishing and Springer, Singapore, 2012).
- 7) Y. Terada, S. Yoshida, O. Takeuchi, and H. Shigekawa: *J. Phys.: Condens. Matter* **22** (2010) 264008.
- 8) S. Loth, M. Etzkorn, C. P. Lutz, D. M. Eigler, and A. J. Heinrich: *Science* **329** (2010) 1628.
- 9) Y. Terada, S. Yoshida, O. Takeuchi, and H. Shigekawa: *Nat. Photonics* **4** (2010) 869.
- 10) Y. Terada, S. Yoshida, O. Takeuchi, and H. Shigekawa: *Adv. Opt. Technol.* **2011** (2011) 510186.
- 11) S. Yoshida, Y. Terada, R. Oshima, O. Takeuchi, and H. Shigekawa: *Nanoscale* **4** (2012) 757.
- 12) S. W. Wu and W. Ho: *Phys. Rev. B* **82** (2010) 085444.
- 13) N. Weiss, H. Zhou, L. Liao, Y. Liu, S. Jiang, Y. Huang, and X. Duan: *Adv. Mater.* **24** (2012) 5782.
- 14) H. Fang, S. Chuang, T. C. Chang, K. Takei, T. Takahashi, and A. Javey: *Nano Lett.* **12** (2012) 3788.
- 15) Q. Wang, K. Zadeh, A. Kis, J. Coleman, and M. Strano: *Nat. Nanotechnol.* **7** (2012) 699.
- 16) Ch. Sommerhalter, Th. W. Matthes, J. Boneberg, P. Leiderer, and M. Ch. Lux-Steiner: *J. Vac. Sci. Technol. B* **15** (1997) 1876.
- 17) M. W. J. Prins, R. Jansen, R. H. M. Groeneveld, A. P. van Gelder, and H. van Kempen: *Phys. Rev. B* **53** (1996) 8090.
- 18) C. Enss, R. Winters, M. Reineremann, G. Weiss, S. Hunklinger, and M. Lux-Steiner: *Z. Phys. B* **99** (1996) 561.
- 19) M. Berthe, S. Yoshida, Y. Ebine, K. Kanazawa, A. Okada, A. Taninaka, O. Takeuchi, N. Fukui, H. Shinohara, S. Suzuki, K. Sumitomo, Y. Kobayashi, B. Grandidier, D. Stievenard, and H. Shigekawa: *Nano Lett.* **7** (2007) 3623.